Int. J. Heat Mass Transfer. Vol. 36, No. 4, pp. 977–988, 1993
Printed in Great Britain

0017–9310/93 $6.00 + 0.00
© 1993 Pergamon Press Ltd

The hydrodynamic stability of a one-dimensional transient buoyancy-induced flow

MATTHEW JOHN M. KRANE†
Digital Equipment Corporation, 100 Minuteman Road, APO2-F2, Andover, MA 01810, U.S.A.

and

BENJAMIN GEBHART
Department of Mechanical Engineering and Applied Mechanics, University of Pennsylvania, Philadelphia, PA 19104-6315, U.S.A.

(*Received* 23 *July* 1991 *and in final form* 21 *April* 1992)

Abstract—Recent experiments have shown that a transient, buoyant, laminar and one-dimensional flow adjacent to a vertical flat surface may become vigorous enough to begin a transition process from laminar to turbulent flow. The disturbance amplification characteristics of such a flow are analyzed using linear stability theory. The Orr–Sommerfeld equations for stream function and temperature disturbances are formulated for an imposed constant and uniform base surface heat flux. These equations are solved for water, $Pr = 6.7$, with a step in surface heat flux from zero to a non-zero value. The temporal amplification of the disturbance components is found as a function of their frequency. The results are plotted on a stability plane which shows that the selective amplification found in steady, downstream-developing buoyancy driven flows also occurs in transients. The new results are shown to be in moderate agreement with recent measurements. Temperature and velocity disturbance profiles across the boundary region are also examined. For the same boundary conditions, the qualitative effect of Pr on the temporal growth of disturbances is also discussed.

1. INTRODUCTION

THE TRANSIENT behavior of laminar buoyancy-induced flows has been extensively studied through analysis and experiment, as this behavior has important applications in many natural and industrial processes. Because many of the applications involved vigorous flows which tend to undergo transition to turbulence, it is useful to examine the initial instabilities leading to that transition in a one-dimensional transient flow.

1.1. *Previous transient buoyancy-induced flow studies*

The first study of a transient buoyancy driven flow [1] concerned an initially quiescent fluid with a flow generated by a step in the temperature of a doubly infinite flat surface, for $Pr = 1$. The assumption was made that the flow was independent of the downstream coordinate, parallel to the plate. This assumption results in heat transfer only by conduction (see Section 2.2). Later studies [2, 3] obtained solutions for an arbitrary Prandtl number and several additional kinds of thermal boundary conditions. Experiments in water [4] with a Mach–Zender interferometer confirmed the one-dimensional flow assumption for short times.

Siegel [5] analyzed a transient buoyancy-induced flow next to a semi-infinite vertical flat plate using approximate profiles suggested by Eckert [6]. Both wall temperature step and wall heat flux step boundary conditions were studied for $Pr = 1$. Siegel identified three regimes during the transient response: (1) purely conductive heat transfer, with a correspondingly one-dimensional flow field; (2) truly transient flow, with all of the terms in the transient Navier–Stokes equations of about the same order; and, (3) the final approach to steady-state, a quasi-static regime. Several experimental studies in air and water [7–10] confirmed these and other theoretical predictions.

Goldstein and Briggs [11] analyzed the flow adjacent to vertical plane and cylindrical surfaces and predicted the length of time the one-dimensional regime is valid, as a function of the distance downstream. The experiments in ref. [4] agreed with this analysis. Brown and Riley [12] reported calculations which predicted a slightly faster penetration rate for the leading edge effect.

1.2. *Linear stability theory applied to buoyancy-induced flow*

There have been many studies of the downstream transition to turbulence in steady buoyancy-induced flows. They have generally shown that this transition in laminar boundary layer flows arises from the pres-

† Present address: Department of Mechanical Engineering, Purdue University, West Lafayette, IN 47907, U.S.A.

NOMENCLATURE

A^*	transient flow vigor parameter, defined in equation (25)
c''	wall thermal capacity [J m^{-2} K^{-1}]
c_r	phase velocity
F	similarity velocity
g	gravitational acceleration [m s^{-2}]
G^*	steady flow vigor parameter, defined in equation (26)
H	similarity temperature
i	$\sqrt{-1}$
k	thermal conductivity [W m^{-1} K^{-1}]
P, p	motion pressure [N m^{-2}]
p'	disturbance motion pressure [N m^{-2}]
Pr	Prandtl number
q''	power dissipation per unit wall area [W m^{-2}]
Q^*	generalized thermal capacity effect
R	ratio defined in equation (36)
s	generalized disturbance temperature
t	temperature [K]
t'	disturbance temperature [K]
U, u	x-velocity [m s^{-1}]
u'	disturbance x-velocity [m s^{-1}]
V, v	y-velocity [m s^{-1}]
v'	disturbance y-velocity [m s^{-1}]
x, y	Cartesian coordinates [m].

Greek symbols

α, β	generalized eigenvalues
α_T	thermal diffusivity [m^2 s^{-1}]
β_T	coefficient of thermal expansion [K^{-1}]
δ	thermal penetration length [m]
η	similarity variable
θ	temperature excess, $t_b - t_\infty$ [K]
ν	kinematic viscosity [m^2 s^{-1}]
ρ	density [kg m^{-3}]
τ	time [s]
ϕ	generalized disturbance streamfunction
ψ'	disturbance streamfunction [m^2 s^{-1}]
Ω^*	generalized time-independent frequency, defined in equation (35).

Subscripts

b	base flow
i	imaginary
r	real
o	reference quantity
∞	ambient and initial.

Other symbols

$-$	dimensional quantities
$'$	η derivative (except where noted)
NSC	neutral stability curve.

ence of initially small disturbances. Experiments have shown that the consequence is the amplification of sinusoidal disturbance components. In the region where the disturbances have small amplitude, linear stability theory has been a very successful model of their downstream behavior. Linear theory assumes disturbances small enough that the higher-order disturbance terms may be neglected. The goal is to determine the behavior of the constituent disturbance components. Will they amplify, decay, or remain the same, as a function of their frequency and the base flow vigor parameter? (This parameter is G^* for two-dimensional steady flows and A^* for one-dimensional transient flows, which are defined in equations (25) and (26).)

The first complete solution which applied linear stability theory to these problems was by Nachtsheim [13]. The buoyancy effect in the disturbance equations, which had been left out in previous studies due to computational difficulties, was retained. Several studies in the next few years refined the method of calculating instability conditions and produced very important results. These results were supported by related experimental work. Knowles and Gebhart [14] found neutral curves over a range of Pr and showed that the calculated eigenfunctions agreed very well with their measurements in silicone oil ($Pr = 7.7$) [14, 15]. These data also confirmed the analytical prediction that the maximum value of the velocity disturbance occurs at the same cross-stream location as the maximum base flow velocity, not at the base flow's point of inflection, as generally predicted by inviscid analysis.

Dring and Gebhart [16] extended the above analysis into the unstable region far downstream of the neutral curve location. It was discovered that, as the vigor parameter G^* increases, an increasingly narrow band of frequencies is more highly amplified than all the rest. This result was confirmed by experiment [17] and by further analysis over a larger range of the vigor parameter and Pr [18]. This selective amplification of frequencies is not found in similar calculations on forced flows, such as the Blausius-type flows, where all disturbances, no matter how low the frequency, eventually decay.

The studies above concerned themselves with the downstream development of disturbances in two-dimensional steady boundary layer flows. An experimental study [19] discovered that the initial developing one-dimensional transient flow, the purely conductive regime discussed previously, may become vigorous enough to begin a transition process before the flow was swept away by the local arrival of the leading edge effect. These data showed that measurable disturbances appear in the one-dimensional flow at times before the arrival of the leading edge effect

predicted [12]. The disturbances also arise at approximately the same time throughout the downstream region of the one-dimensional flow. That is, the downstream distance seems to have no influence on the appearance and temporal growth of these disturbances; they are also one-dimensional. A fast Fourier transform analysis of these data indicated that these disturbance frequencies are concentrated in a narrow band around the same characteristic frequency as in a similar two-dimensional steady flow. This remarkable result is developed further in Joshi and Gebhart [19].

The present study concerns this region of one-dimensional transient instability and transition. Applying linear stability theory, a stability plane is generated for $Pr = 6.7$ and compared to available data. Neutral curves are also found for a range of Pr. The resulting eigenfunctions for $Pr = 6.7$ are compared to their counterparts in steady two-dimensional flows.

2. PROBLEM FORMULATION

2.1. *Full equations*

The analysis will be of the flow resulting from an instantaneous change in the thermal boundary condition of a doubly infinite vertical flat surface at t_∞ in contact with a quiescent fluid, also initially at t_∞. The type of change considered here is a step from no surface energy input to an input at a uniform, constant and finite level, q''.

The analysis is based on the two-dimensional Navier–Stokes equations for buoyancy-induced flows. The buoyancy force is in the vertical direction only, i.e. parallel to the surface (see Fig. 1). The energy equation also arises, in which the viscous dissipation and pressure work terms are neglected. The two Boussinesq approximations are applied. These assumptions are that the density is linearly related to temperature and that the density change due to temperature is a small fraction of the ambient fluid density. All fluid properties other than density in the buoyancy term are taken to be constant and uniform. The general two-dimensional equations for velocity, temperature and the motion pressure are:

$$\frac{\partial U}{\partial x}+\frac{\partial V}{\partial y}=0 \tag{1}$$

$$\frac{\partial U}{\partial \tau}+U\frac{\partial U}{\partial x}+V\frac{\partial U}{\partial y}=\nu\nabla^2 U-\frac{1}{\rho}\frac{\partial P}{\partial x}+g\beta_T(t-t_\infty) \tag{2}$$

$$\frac{\partial V}{\partial \tau}+U\frac{\partial V}{\partial x}+V\frac{\partial V}{\partial y}=\nu\nabla^2 V-\frac{1}{\rho}\frac{\partial P}{\partial y} \tag{3}$$

$$\frac{\partial t}{\partial \tau}+U\frac{\partial t}{\partial x}+V\frac{\partial t}{\partial y}=\alpha_T\nabla^2 t \tag{4}$$

$$U(x,0,\tau)=U(x,\infty,\tau)=U(x,y,0)=0$$

$$V(x,0,\tau)=V(x,\infty,\tau)=V(x,y,0)=0$$

$$t(x,\infty,\tau)-t_\infty=t(x,y,0)-t_\infty=0$$

$$\frac{\partial t}{\partial y}(x,0,\tau)+\frac{q''}{k}=0. \tag{5}$$

Equations (1)–(4) are the conservation of mass, momentum and energy.

The velocity, temperature and pressure are each taken as a sum of the base flow quantity and a small disturbance

$$U=U_b+u',\quad V=V_b+v'$$

$$t=t_b+t',\quad P=P_b+p'. \tag{6}$$

In the analysis of the disturbance behavior, the base flow is found first. The disturbances are then postulated and are superimposed on the base flow solution to determine the time dependent disturbance behavior.

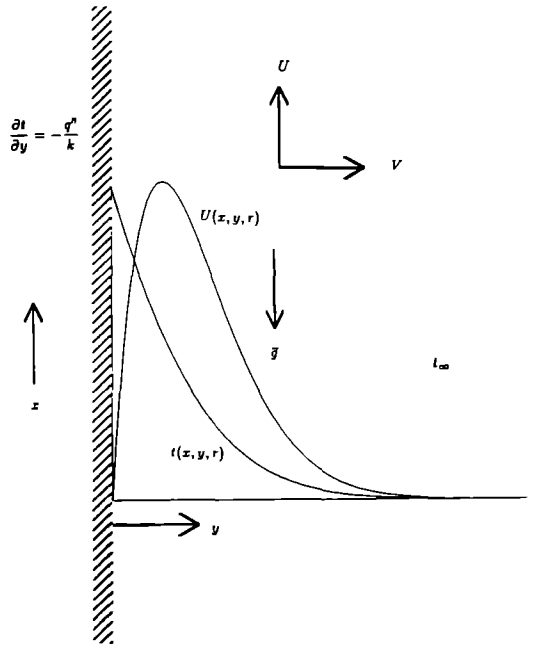

FIG. 1. System geometry.

2.2. *Base flow*

The mechanism to be analyzed is the initial transient regime found in experimental, numerical and analytical studies, most recently in ref. [19]. The transient base flow is a solution to equations (1)–(5). In this one-dimensional regime, there is no variation in the x-direction of the base flow quantities. The continuity equation (1) becomes:

$$\frac{\partial V_b}{\partial y}=0 \quad \text{or} \quad V_b=V_b(\tau) \quad \text{only.} \tag{7}$$

Applying the boundary condition for V_b, it is seen that $V_b = 0$ everywhere and for all time. This result and the x-independence of the base quantities reduce equations (2)–(5) to

$$\frac{\partial U_b}{\partial \tau} = \nu \frac{\partial^2 U_b}{\partial y^2} + g\beta_T \theta \tag{8}$$

$$0 = \frac{\partial P_b}{\partial y} \tag{9}$$

$$\frac{\partial \theta}{\partial \tau} = \alpha_T \frac{\partial^2 \theta}{\partial y^2} \tag{10}$$

$$U_b(0, \tau) = U_b(\infty, \tau) = U_b(y, 0) = 0$$

$$\theta(\infty, \tau) = \theta(y, 0) = 0$$

$$\frac{\partial \theta}{\partial y} + \frac{q''}{k} = 0 \quad (\tau > 0). \tag{11}$$

No base flow convective terms arise in these equations. The only remaining transfer mode of heat and momentum transfer is diffusion.

The existence of a similarity form for these equations may be confirmed using a transformation group method [20]. This method produces the forms of the independent and dependent variables for the similarity solution. If the non-dimensional similarity variable is defined as

$$\eta = \frac{y}{\sqrt{(4\alpha_T \tau)}} \tag{12}$$

the velocity and temperature fields may be written

$$U_b(\eta, \tau) = U_0(\tau) F(\eta) \quad \text{and} \quad \theta(\eta, \tau) = t_0(\tau) H(\eta). \tag{13}$$

The solutions for $Pr \neq 1$ [2], arranged in a convenient manner, are

$$U_0 = \frac{g\beta_T q'' \tau (\alpha_T \tau)^{1/2}}{k}$$

$$F = \frac{8}{1 - Pr}\left(i^3 \operatorname{erfc}(\eta) - i^3 \operatorname{erfc}\left(\frac{\eta}{\sqrt{(Pr)}}\right)\right)$$

$$t_0 = \frac{q''(\alpha_T \tau)^{1/2}}{k}$$

$$H = \frac{2}{\sqrt{\pi}} \exp(-\eta^2) - 2\eta \operatorname{erfc}(\eta). \tag{14}$$

(The quantity i^3 erfc is a repeated integral of the complimentary error function.) Note that the Prandtl number appears in the velocity rather than in the temperature solution, where it is usually expected. This change is caused by the use of a thermally based length scale ($2\sqrt{(\alpha\tau)}$), rather than the usual one based on viscosity. This flow is driven by a diffusion of heat which is unaffected by fluid motion. Therefore, the coupling between momentum and heat transfer should only appear in the momentum equation. This situation is analogous to forced convection, in which the flow is not affected by heat transfer and the only coupling (and, therefore, Pr) is in the energy equation.

2.3. *Disturbances*

Having specified the base flow, equation (6) is substituted into equations (1)–(5). Recall that $V_b = 0$ and $dP_b/dy = 0$, and that the base flow is independent of x. Assuming that the disturbances remain much smaller than the base flow, e.g. $U_b \gg u'$, and subtracting out the purely base flow terms, the conservation equations, in terms of the disturbances, are:

$$\frac{\partial u'}{\partial \tau} + U_b \frac{\partial u'}{\partial x} + v' \frac{\partial U_b}{\partial y} = \nu \nabla^2 u' - \frac{1}{\rho} \frac{\partial p'}{\partial x} + g\beta_T t' \tag{15}$$

$$\frac{\partial v'}{\partial \tau} + U_b \frac{\partial v'}{\partial x} = \nu \nabla^2 v' - \frac{1}{\rho} \frac{\partial p'}{\partial y} \tag{16}$$

$$\frac{\partial t'}{\partial \tau} + U_b \frac{\partial t'}{\partial x} + v' \frac{\partial \theta}{\partial y} = \alpha_T \nabla^2 t'. \tag{17}$$

The form of the stream function and temperature disturbances is postulated to be the first mode of a Fourier series solution to these equations:

$$\psi' = U_0 \delta \phi(\eta) \exp[i(\bar{\alpha}x - \bar{\beta}\tau)] \tag{18}$$

$$t' = t_0 s(\eta) \exp[i(\bar{\alpha}x - \bar{\beta}\tau)] \tag{19}$$

where $\psi'_y = u'$ and $-\psi'_x = v'$, and ϕ and s are complex in general. Using the *ad hoc* approximation that the system is quasistatic, that is, the growth rate of the disturbances is much greater than the growth rate of the base flow [21], the τ dependence of the base flow in equations (15)–(17) is relatively weak and the solution can be Fourier analyzed in x and τ. This simplification is analogous to the parallel flow approximation made in steady boundary layer flows [22]. The two disturbances have the same wavelength and frequency due to the coupling of the velocity and temperature fields.

The eigenvalues, $\bar{\alpha}$ and $\bar{\beta}$, are also both complex, in general

$$\bar{\alpha} = \bar{\alpha}_r + i\bar{\alpha}_i \tag{20}$$

$$\bar{\beta} = \bar{\beta}_r + i\bar{\beta}_i. \tag{21}$$

The real part of $\bar{\alpha}$ is the wave number, $\mathrm{Re}(\bar{\alpha}) = 2\pi/\lambda$, and $\bar{\alpha}_i$ is the spatial amplification rate. $\mathrm{Re}(\bar{\beta}) = 2\pi f$ is the physical frequency of the disturbances, while $\mathrm{Im}(\bar{\beta})$ is the temporal amplification rate.

In most stability analyses of two-dimensional downstream developing steady base flows, there is no temporal amplification, that is, $\bar{\beta}_i = 0$. Extensive experimentation has shown that such disturbances grow in magnitude only with downstream distance. However, the present study follows the recent observations [19] in one-dimensional transients. Figure 2 shows the appearance of the disturbances at different generalized downstream positions, X, as a function of generalized time, τ. The local sensor data indicated that, during the one-dimensional regime, disturbances often arise and grow in time, amplifying simultaneously over the entire one-dimensional region. Therefore, $\bar{\beta}_i \neq 0$, in general, and $\bar{\alpha}_i = 0$, always.

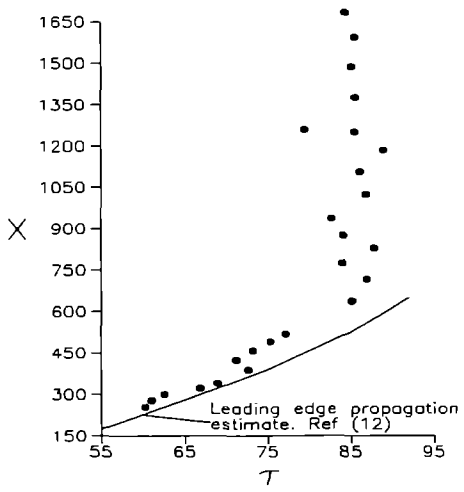

FIG. 2. Nondimensional times for first observed disturbances at various downstream locations [19].

The generalizations of the disturbance-related eigenvalues are:

$$\bar{\alpha} = \frac{\alpha}{\delta}$$

$$\bar{\beta} = \beta\left(\frac{U_0}{\delta}\right)$$

$$\delta = (4\alpha_T\tau)^{1/2}. \tag{22}$$

Again using a quasistatic approximation, the time derivatives of U_0, t_0 and δ are neglected and equations (18), (19) and (22) are applied to (15)–(17). The two momentum equations are cross differentiated and their difference is found to eliminate the pressure terms. The result, along with the disturbance energy equation, is:

$$\left(F-\frac{\beta}{\alpha}\right)(\phi''-\alpha^2\phi)-F''\phi = \frac{1}{i\alpha A^*}\left[\phi^{iv}-2\alpha^2\phi''+\alpha^4\phi+\left(\frac{4}{Pr}\right)s'\right] \tag{23}$$

$$\left(F-\frac{\beta}{\alpha}\right)s-H'\phi = \frac{1}{i\alpha A^* Pr}[s''-\alpha^2 s] \tag{24}$$

where

$$A^* = \frac{U_0\delta}{\nu} = \frac{2g\beta q''\alpha_T\tau^2}{k\nu}. \tag{25}$$

These equations for a one-dimensional transient buoyancy-induced flow are in the same form as for the two-dimensional downstream developing flow, with three exceptions. The parameter $A^*(\tau)$ appears instead of the modified Grashof number

$$G^*(x) = 5\left(\frac{Gr^*}{5}\right)^{1/5} = 5\left(\frac{g\beta q'' x^4}{5k\nu}\right)^{1/5}. \tag{26}$$

The $(4/Pr)$ coefficient appears in front of the thermal coupling term, rather than the coefficient of unity found in the downstream developing flow formulation. This result is explained by the same reasoning as the position of Pr in the base flow solutions, i.e. a thermal rather than a viscous length scale has been used. Finally, the base flow quantities, F, F'' and H', are the one-dimensional transient base flow, rather than the two-dimensional steady state boundary layer solutions.

The disturbance boundary conditions are as follows. From the no-slip condition and assuming an impermeable wall

$$\phi(0) = \phi'(0) = 0. \tag{27}$$

Because the disturbance energy must be finite

$$\phi(\eta \Rightarrow \infty) = \phi'(\eta \Rightarrow \infty) = s(\eta \Rightarrow \infty) = 0. \tag{28}$$

The thermal condition at the wall is generally more complicated because any thermal capacity in the wall material may have an important effect on the temperature disturbance amplitude there. The general flux boundary condition, including a surface thermal capacity per unit area of c'', is

$$q'' = c''\frac{\partial\theta}{\partial\tau} - k\frac{\partial\theta}{\partial y}. \tag{29}$$

This condition yields the following disturbance condition at $\eta = 0$:

$$s(0) = \frac{i}{A^* Q^* \beta}s'(0) \tag{30}$$

where $Q^* = (vc''/k\delta)$. For the surface flux condition analyzed here, the thermal capacity effect is assumed to be negligible, for both the development of the disturbances and the base flow. This assumption is generally true in the case of thin surface elements in liquids. The surface used by Joshi and Gebhart [19] had a Q^* between 0.024 and 0.031 in the region in which disturbances were first recorded. The thermal disturbance boundary condition at the surface is taken as

$$Q^* \Rightarrow 0 \quad \text{and} \quad s'(0) = 0. \tag{31}$$

2.4. *Numerical solution*

The system defined by equations (23) and (24), with the boundary conditions (27), (28) and (31), is solved by the method of Heiber and Gebhart [18]. This procedure expresses the solutions, ϕ and s, each as linear combinations of three integrals, the inviscid $(\phi, s)_1$, the viscous uncoupled $(\phi, s)_2$ and the viscous coupled $(\phi, s)_3$:

$$\phi = B_1\phi_1 + B_2\phi_2 + B_3\phi_3 \tag{32}$$

$$s = B_1 s_1 + B_2 s_2 + B_3 s_3. \tag{33}$$

Because it is awkward to use the boundary conditions at infinity, equation (28), the first order asymp-

totic solutions for large η are found for the six integrals in equations (32) and (33)

$$\phi_1 = \exp(-\alpha\eta)$$

$$\phi_2 = \exp[-\alpha(\alpha^2 - iA^*\beta)^{1/2}\eta]$$

$$\phi_3 = \exp[-\alpha(\alpha^2 - iA^*\beta\, Pr)^{1/2}\eta]$$

$$s_1 = s_2 = 0$$

$$s_3 = \frac{(\beta A^*)^2 Pr(1-Pr)}{(\alpha^2 - iA^*\beta\, Pr)^{1/2}}\phi_3. \tag{34}$$

To solve equations (23) and (24) for a given Pr, the values of two of the four parameters (A^*, α_r, β_r, β_i) are assumed. The other two are initially guessed and are to be changed iteratively toward convergence. The equations are integrated three times by a fourth order Hammings modified predictor–corrector method, each time using a different integral, $(\phi, s)_1$, $(\phi, s)_2$ or $(\phi, s)_3$ from equation (34), for the boundary conditions at infinity. Because this system has homogeneous equations and boundary conditions, it is an eigenvalue problem and the solution is known only to an arbitrary constant. Therefore, B_1 can be conveniently set to unity. Then B_2 and B_3 are found from the velocity boundary conditions, equation (27). Using three constants, the value of $s'(0)$ is determined. This set of three integrations is repeated twice, first varying one guessed parameter slightly, then the other. These results are then used by a finite difference Nachtsheim–Swigert method [23] to calculate new guesses for the two parameters. This process is continued until $s'(0) < |10^{-4}|$.

The outer boundary at which equations (34) are used is called η_{edge}. This value and the step size, $\Delta\eta$, are found by trial and error, using as small an η_{edge} and as large a $\Delta\eta$ as possible without significantly altering any converged results.

3. RESULTS AND DISCUSSION

3.1. *Eigenvalues and disturbance amplification*

The eigenvalues are found by the iterative process described previously and are known to at least four significant digits. A plot of β_r (frequency) vs A^* with constant β_i (temporal amplification rate) contours, for $s'(0) = 0$ and $Pr = 6.7$, is shown in Fig. 3. This stability plane shows the temporal amplification rates of the disturbances as functions of frequency, β_r. The vigor parameter, $A^*(\tau)$, has the same role here in the Orr–Sommerfeld equations as does $G^*(x)$ in two-dimensional buoyancy driven convection and Re (x) in forced flows.

The first disturbance component to be amplified crosses the $\beta_i = 0$ curve, the location of neutral stability and $A^* = 22.6$, at about $\beta_r = 0.01$. This curve is calculated up to a maximum β_r of 0.0617, at $A^* = 377$. Beyond this location a converged solution could not be found with the present method, due to large differences in the order of magnitude of the six integrals in equations (32) and (33). For the lower frequencies, $\beta_r < 0.02$, calculations were carried out far enough in A^* to include experimental data from [19]. At higher frequencies, calculations were carried out as far as possible, within the limitation mentioned above. Closure of three higher amplification rate contours, β_i, are shown in the region calculated. Although not shown in Fig. 3, the $\beta_i = 0.001$ contour closes at $A^* \approx 4000$.

Inviscid analysis, which solves the Orr–Sommerfeld equations at $A^* \Rightarrow \infty$, predicts that laminar flows with a point of inflection in the velocity profile are unstable

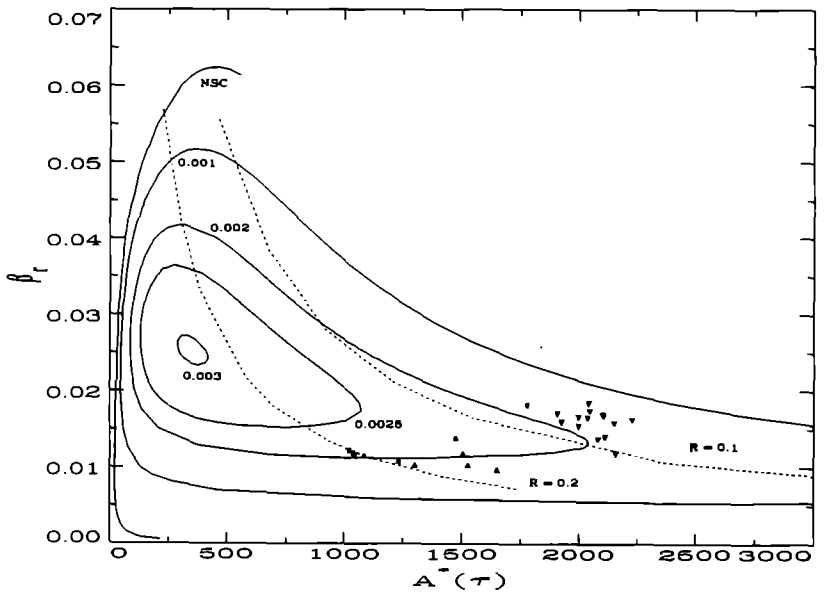

FIG. 3. Stability plane for $Pr = 6.7$, uniform flux surface, $s'(0) = 0$ (· · · ·, constant R; – – – –, constant β_i; ▲, disturbances due to leading edge effect; ▼, disturbances in one-dimensional regime [19]).

over a finite range of frequency, β_r, in the limit of infinite A^* [24]. The base flow studied here has such a point of inflection, so the neutral curve, $\beta_i = 0$, should approach some non-zero, finite value for infinite A^*. This non-closure of the neutral stability curve would indicate that a certain range of frequencies will be continuously amplified for all subsequent times, that is, for all values of A^*, as long as the disturbance amplitudes are small enough that the linear approximation is valid.

There are two general components of disturbance growth in this flow. One is the growth of disturbance amplitudes, ψ' and t', due to the temporal growth of the base flow quantities, U_0, δ and t_0. This effect is not of interest here because it does not cause the disturbances to grow or decay relative to the base flow and therefore does not contribute to transition. This effect is removed from the analysis in the development of equations (23) and (24). The second type of disturbance growth or decay is the temporal change in the exponential terms in equations (18) and (19). These terms are a measure of the rate of change of disturbance amplitudes relative to the base flow. This effect is modelled by the Orr–Sommerfeld equations and it is of interest because transition occurs only if the disturbance amplitude grows more rapidly than the base flow.

The only experimental data available for this transient configuration and flow regime are those given by Joshi and Gebhart [19]. From their plots of disturbance behavior through time during the one-dimensional regime, it appears that the principal disturbance frequency component remains approximately constant at later times. However, in Fig. 3, the generalized frequency, $\beta_r = \bar{\beta}_r(U_0/\delta)$, is a function of time. The best way to examine the behavior of a disturbance frequency component through time is along a constant physical frequency path, Ω^*, where

$$\Omega^* = \beta_r(A^*)^{1/2}. \tag{35}$$

This transformation eliminates the time dependence in the nondimensionalized physical frequency, Ω^*. A plot of Ω^* vs A^*, with constant β_i contours, is shown in Fig. 4.

The neutral curve in Fig. 4 shows that the first calculated disturbance frequency component becomes unstable at $A^*_{crit} = 22.6$ and $\Omega^* = 0.048$. This formulation predicts that this is the first disturbance component to be amplified. However, Fig. 4 shows that this component is not the most highly amplified at later times. Much more highly amplified components are found at higher frequencies for example, $\Omega^* \approx 0.60$ appears to be the most significantly amplified, or characteristic, frequency after $A^* \approx 1500$. This property also appears in the two-dimensional steady flows [16].

Naturally arising disturbance data, from Joshi and Gebhart [19], are plotted on Figs. 3 and 4. These points are seen to be in two distinct groups. The first group arises at lower A^* and corresponds to the ten data points in Fig. 2 which lie along the solid curve. These disturbances, ▲ in the figures, arise approximately at the same time as the theoretical prediction of the arrival of the leading edge effect [12]. Such disturbances apparently do not arise by purely one-dimensional mechanisms and they are not modelled by the analysis here. On the other hand, the majority of these measured frequencies do lie very close to the

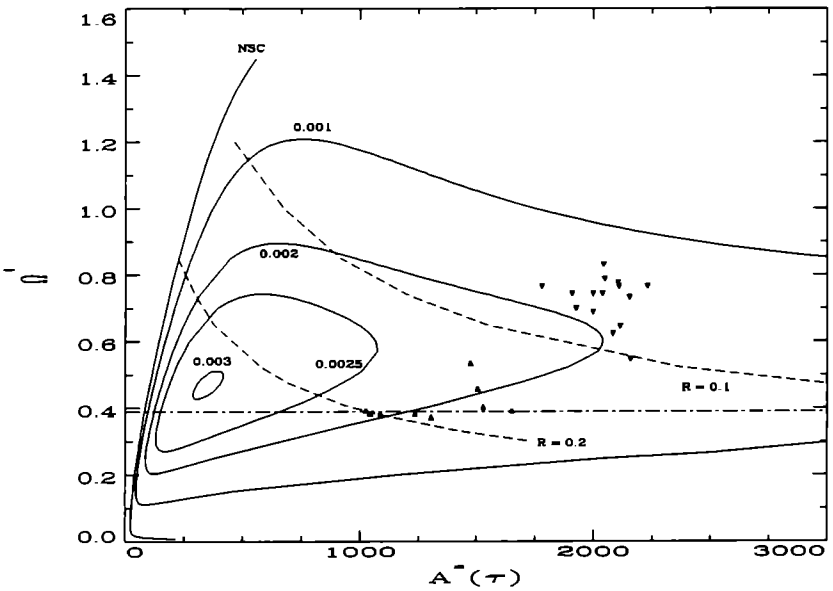

FIG. 4. Stability plane for $Pr = 6.7$, uniform flux surface, $s'(0) = 0$ (– – –, constant R; – · – · –, frequency of disturbances associated with leading edge effect; ▲, disturbances due to leading edge effect; ▼, disturbances in one-dimensional regime [19]).

particular frequency of $\Omega^* = 0.39$. The other two data points of the leading edge effect which do not occur at this frequency did not correlate in terms of the heat flux, the downstream position at which they were measured or the time at which they arose.

The second group of measured disturbance frequencies, the points ▼, arose purely on one-dimensional transient regions of the flow, downstream of the propagating leading edge effect. The frequencies are higher than the calculated most favored frequency ($\Omega^* \approx 0.6$). Figure 3 appears to have better agreement with these data than Fig. 4. However, it must be remembered that β_r is time dependent, while Ω^* is not. Because the physical frequencies appear to be time independent during the time in which they were measured, Fig. 4 presents a clearer picture of the temporal amplification of particular frequency components.

There are several reasonable explanations why these data do not fall as close to the predicted characteristic frequency as do comparisons of data and calculations for steady, downstream developing boundary layer flows. For example, the principal physical disturbance frequency actually may vary in time. The experimental data in ref. [19] capture only two or three full periods of the disturbances, between the time of their appearance and the time of the arrival of the leading edge effect. This effect terminates the one-dimensional regime. While the present analysis uses the idealization of an infinite surface with no leading edge, the experiments correspond to finite surfaces. Therefore, the period in which data may be collected is limited. There are not sufficient data to indicate if the frequency might change over longer times for larger disturbance amplitudes.

Another possible cause of the discrepancy is the applicability of the quasistatic approximation used in the analysis. This approximation is analogous to the parallel flow approximation, which is commonly and successfully used in two-dimensional flows. A quasistatic analysis is appropriate if it can be shown that the acceleration of the flow is small relative to the temporal growth of the disturbances. As an indication of these relative accelerations, the ratio of the time derivatives of the base and disturbance velocities, R, is

$$R = \left| \frac{\partial \ln U_b}{\partial \tau} \Big/ \frac{\partial \ln u'}{\partial \tau} \right| \ll 1. \tag{36}$$

Values of R are shown in Table 1 for four different values of Ω^*, over a range of A^*. The numerator above is evaluated from the base flow solution in Section 2.2 for the conditions of the experimental data [19]. The denominator was calculated from the results given here. Some resulting R values are plotted on Figs. 3 and 4. It is seen in these figures that the approximation is not valid for low values of frequency or A^*. It is, however, valid in the region near the experimental data. Therefore, the position of the β_i contours, especially the lower frequency section of the neutral curve, are not known accurately.

Table 1. Values for R for $Pr = 6.7$, uniform flux surface, $s'(0) = 0$

	Ω^*			
A^*	0.120	0.522	0.738	1.1
NSC	1.640	0.419	0.251	0.129
500	0.819	0.215	0.155	0.105
1000	0.614	0.153	0.110	0.074
1500	0.514	0.125	0.090	0.061
2000	0.451	0.108	0.078	—
2400	0.422	0.099	0.071	—

Another important question is the effect of the Prandtl number, Pr, on the temporal occurrence of instability and disturbance growth. It appears twice in the Orr–Sommerfeld equations used here, in the coefficient for the thermal diffusion term and in the thermal coupling term. In the steady boundary layer flows [14], the effect of the Pr occurs only in the diffusion term. There, increasing Pr stabilizes the flow, that is, the neutral curve lies at larger values of the vigor parameter, G^*. The same effect arises in these transients, as seen in Fig. 5, at higher frequencies. Of course, the positions of these neutral curves are not known exactly due to the inapplicability of the quasistatic approximation. However, since the positions are more accurately known at high Ω^* and because the relative positions of the neutral curves should indicate general shifts in the other β_i contours, it is not unreasonable to draw some qualitative conclusions from these results.

The increasing stabilization with higher Pr is due to the corresponding decrease in the maximum value of $F(\eta)$, the base flow velocity, as seen in Fig. 6. It is this velocity, with the temperature coupling, which drives disturbance growth. The base flow similarity temperature field, H, is independent of the changes in Pr, see equation (14). The qualitative effect of Pr on the behavior of the neutral curve is the same in the steady flow [14], where the coefficient of the coupling term is unity and therefore not dependent on Pr. In transients, it is $4/Pr$. The values of this coefficient which arise here are 5.7–0.6, for $0.7 < Pr < 6.7$. Apparently this variable coefficient does not alter significantly that behavior, at least when it is of order one.

3.2. *Eigenfunctions*

Another important result of this analysis is the distribution of the disturbance eigenfunctions. These complex functions are plotted as real disturbance velocity and temperature amplitudes, normalized by their maximum values

$$\frac{u'}{u'_{max}} = \frac{\sqrt{(\mathrm{Re}\,(\phi')^2 + \mathrm{Im}\,(\phi')^2)}}{(\sqrt{(\mathrm{Re}\,(\phi')^2 + \mathrm{Im}\,(\phi')^2)})_{max}} \tag{37}$$

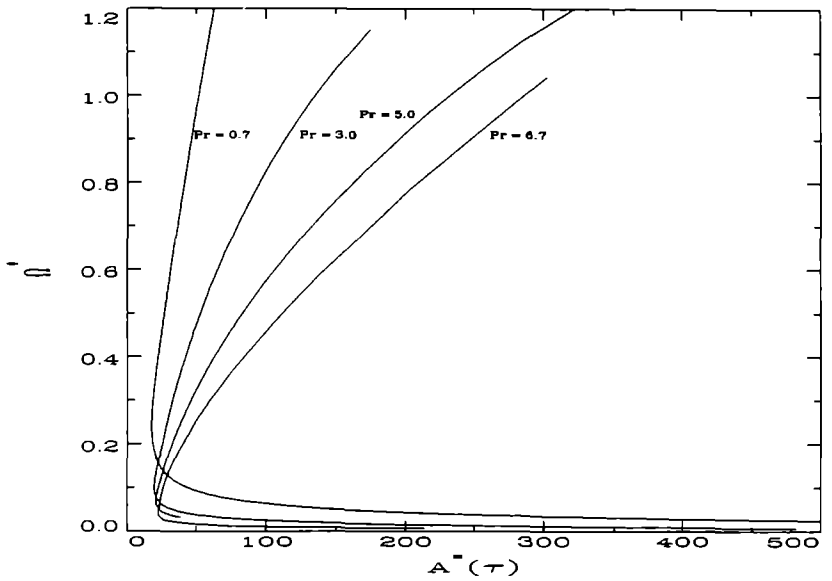

FIG. 5. Neutral stability curves for various Pr, uniform surface flux, $s'(0) = 0$.

$$\frac{t'}{t'_{\max}} = \frac{\sqrt{(\mathrm{Re}\,(s)^2 + \mathrm{Im}\,(s)^2)}}{(\sqrt{(\mathrm{Re}\,(s)^2 + \mathrm{Im}\,(s)^2)})_{\max}}. \tag{38}$$

Profiles of $u'/u'_{\max}$ and $t'/t'_{\max}$ are shown in Figs. 7 and 8, for several values of A^* and Ω^*. The location of the maximum base velocity, the point of inflection in the base velocity and the edges of both the base flow thermal and velocity boundary regions are also marked on these plots by vertical lines along the abscissas.

Inviscid theory suggests that the maximum of the disturbance amplitude should arise at the inflection point of the base velocity [24]. As seen in the figures, the maximum disturbance velocity amplitude at the neutral stability condition occurs between this point and the point of maximum base velocity. As A^* increases, the flow will tend toward an inviscid limit. The peaks for the higher Ω^* are seen to move toward the point of inflection, as expected. Another effect of increasing A^* is a decline in the relative amplitude of the outside peak of the velocity profile, compared to the primary peak. This decrease arises as viscous friction, the principal remaining force outside the base and disturbance temperature boundary regions, becomes relatively less important as A^* increases. In Fig. 7(b), where $\Omega^* = 1.1$, a third peak appears inside

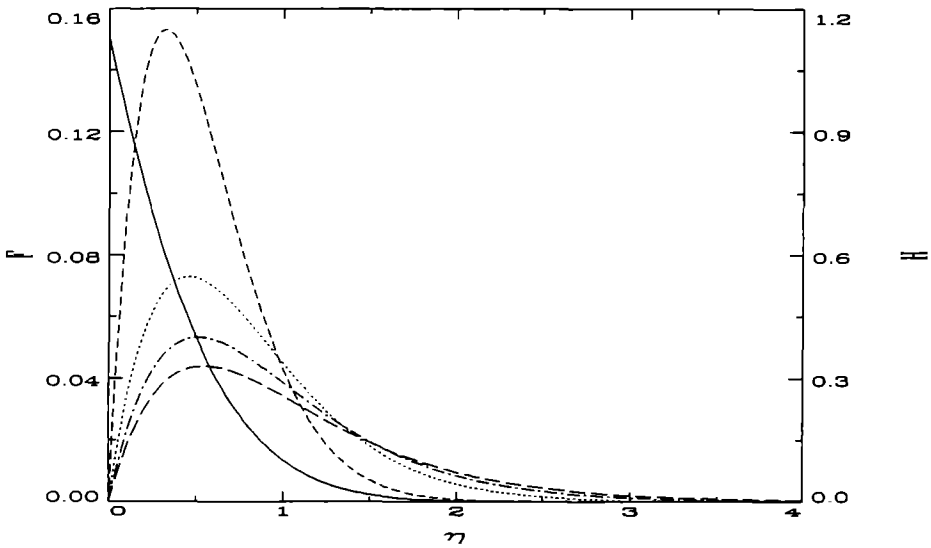

FIG. 6. Base flow velocity and temperature profiles for uniform surface flux condition (----, H (all Pr); – – –, F ($Pr = 0.7$); · · · ·, F ($Pr = 3.0$); – · – · –, F ($Pr = 5.0$); ———, F ($Pr = 6.7$)).

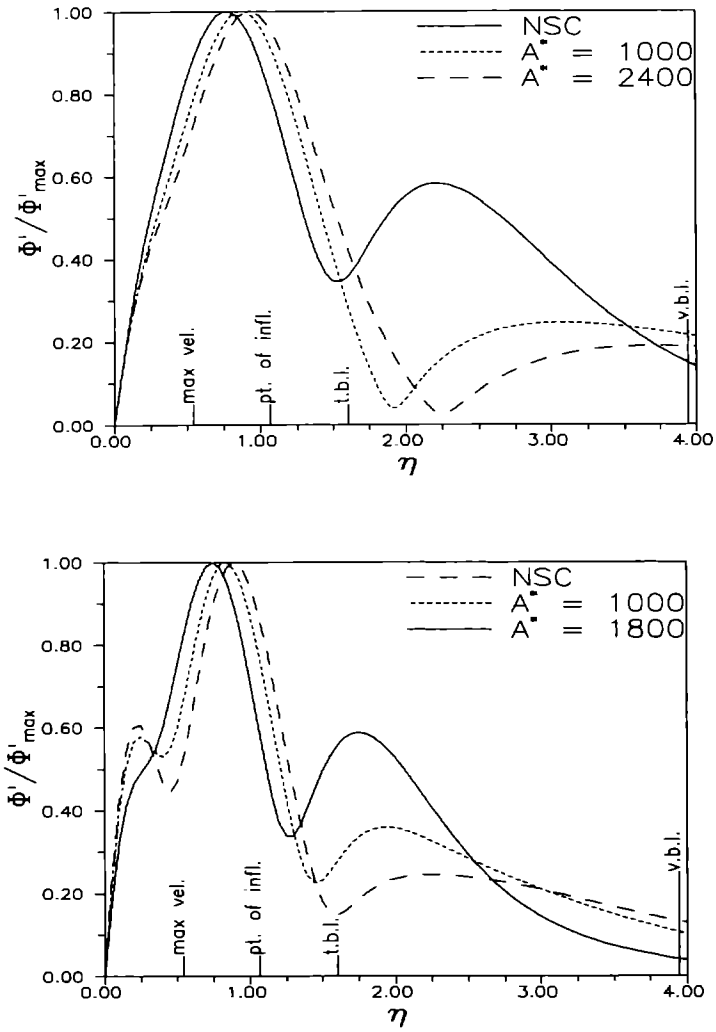

FIG. 7. Disturbance velocity amplitudes: (a) $\Omega^* = 0.522$; (b) $\Omega^* = 1.1$.

the primary peak. It becomes more distinct with larger A^*. In Fig. 7(a), for $\Omega^* = 0.522$, the profile for the highest value of A^* begins to show a change in slope inside of the main peak. This trend indicates the beginnings of a similar peak. This change is correlated with a change in phase velocity

$$c_r = \frac{\beta_r}{\alpha_r} \tag{39}$$

as seen in Table 2. The phase velocity decreases from some peak value at low A^*, along all three constant Ω^* curves shown in the table. As c_r decreases, the third peak begins to appear in Fig. 7(a), $c_r = 0.047$. It becomes more and more distinct as c_r decreases further along the $\Omega^* = 1.1$ line, see Fig. 7(b).

The shapes of most of the disturbance temperature profiles remain of about the same form, over a range of Ω^* and A^*. There are two exceptions. The first is the thickness of the thermal disturbance boundary region, which decreases with higher A^* and Ω^*. The second is the value of $s(0)$, the thermal disturbance amplitude at the surface. The boundary condition applied there is $s'(0) = 0$. However, as Ω^* increases, amounting to an increase in β_r, or as A^* increases, $s(0)$ in equation (29) begins to approach the value it would have if Q^* was large, i.e. $s(0) = 0$. Figures 8(a) and (b) show that for higher A^* and Ω^*, $s(0)$ decreases toward zero.

4. CONCLUSIONS

Using linear stability theory, the equivalent of the Orr–Sommerfeld equations for the stream function and temperature perturbations in a transient one-dimensional buoyancy driven flow have been formulated. The boundary condition which initiates the flow is a constant and uniform heat flux applied to the surface for time greater than zero. The equations have been solved for the flux condition for $Pr = 6.7$, assuming $s'(0) = 0$. This assumption is appropriate for thin surfaces with low thermal capacity relative to the adjacent fluid, as for water. Two types of stability

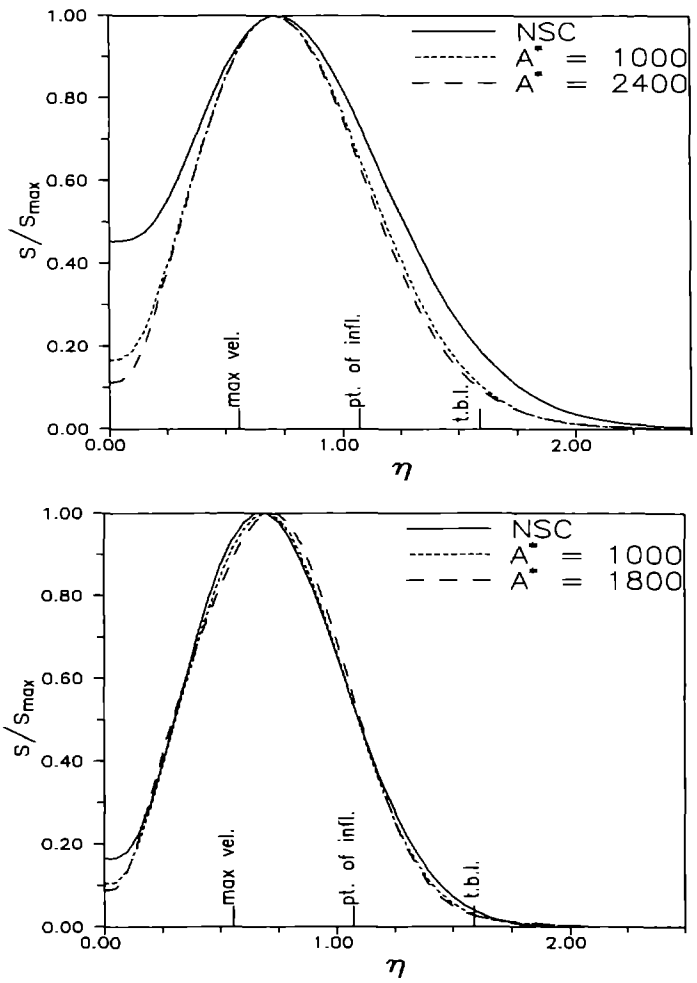

FIG. 8. Disturbance temperature amplitudes: (a) $\Omega^* = 0.522$; (b) $\Omega^* = 1.1$.

Table 2. Phase velocity c_r, for $Pr = 6.7$, uniform flux surface, $s'(0) = 0$

	Ω^*		
A^*	0.120	0.522	1.1
NSC	0.0669	0.0476	0.0450
500	0.0718	0.0484	0.0445
1000	0.0705	0.0478	0.0435
1500	0.0693	0.0475	0.0428
2000	0.0686	0.0472	—
2400	0.0680	0.0470	—

planes are given. They cover the time at which experimental results apply and also frequencies over a band higher and lower than those measured. Profiles of disturbance temperature and velocity show both the effect of frequency, Ω^*, and of the vigor parameter, A^*, on both the shapes of the curves and the values of the surface amplitude, $s(0)$. Then, using the same boundary conditions, the neutral curves for several Pr have been found. The neutral curves indicate a higher degree of stability with larger Pr. These results also show that the Pr dependence in the thermal coupling term does not have a large qualitative effect on the neutral stability condition.

While the frequency data do not have the extremely close agreement with the calculated characteristic frequency found in the steady downstream developing boundary layer flows, the available experimental results [19] are in reasonable agreement with the analysis, despite the fact that the quasistatic approximation is not valid at low frequency or low A^*. The data is based on a very few disturbance oscillations before the leading edge effect arrives and the behavior over longer time periods has not been measured. Useful future measurements should determine disturbance frequencies at higher A^*, as well as the actual disturbance amplitude distributions across the boundary region. Also, improved methods of calculation could be used to predict the behavior at higher A^*, where the quasistatic approximation is more applicable. This formulation provides a reasonable, first order method of predicting disturbance growth in a transient one-dimensional buoyancy-induced flow.

Acknowledgements—The authors would like to thank Digital

Equipment Corporation for use of its computer facilities at its Andover site. The first author would also like to thank Dr Robert Brewster for many useful discussions during the course of this work. This study was supported by the National Science Foundation (Grant CTS-8913393).

REFERENCES

1. C. R. Illingworth, Unsteady laminar flow of a gas near an infinite flat plate, *Proc. Camb. Phil. Soc.* **46**, 603–613 (1960).
2. J. A. Schetz and R. Eichhorn, Unsteady natural convection in the vicinity of a doubly infinite flat plate, *J. Heat Transfer* **84**, 334–338 (1962).
3. E. R. Menold and K.-T. Yang, Asymptotic solutions for unsteady laminar free convection on a vertical plate, *J. Appl. Mech.* **84**, 124–126 (1962).
4. R. J. Goldstein and E. R. G. Eckert, The steady and transient free convection on a uniformly heated vertical plate, *Int. J. Heat Mass Transfer* **1**, 208–218 (1960).
5. R. Siegel, Transient free convection from a vertical flat plate, *J. Heat Transfer* **80**, 347–359 (1958).
6. E. R. G. Eckert, *An Introduction to the Transfer of Heat and Mass*. McGraw-Hill, New York (1950).
7. J. H. Martin, An experimental study of unsteady state natural convection from vertical plates, M.Sc. thesis, Cornell University, Ithaca, New York (1961).
8. H. Lurie and H. A. Johnson, Transient pool boiling of water on a vertical surface with a step in heat generation, *J. Heat Transfer* **84**, 217 (1962).
9. B. Gebhart and D. E. Adams, Measurements of transient natural convection on flat vertical surfaces, *J. Heat Transfer* **85**, 25 (1963).
10. B. Gebhart, R. P. Dring and C. E. Polymeropolous, Natural convection from vertical surfaces, the convective transient regime, *J. Heat Transfer* **89**, 53 (1967).
11. R. J. Goldstein and D. G. Briggs, Transient free convection about vertical plates and circular cylinders, *J. Heat Transfer* **86**, 490–500 (1964).
12. S. N. Brown and N. Riley, Flow past a suddenly heated vertical plate, *J. Fluid Mech.* **59**, 225–237 (1973).
13. P. Nachtsheim, Stability of free-convection boundary layers flows, NASA TN D-2089 (1963).
14. C. P. Knowles and B. Gebhart, The stability of the laminar natural convection boundary layer, *J. Fluid Mech.* **34**, 657–686 (1968).
15. C. P. Knowles and B. Gebhart, An experimental investigation of the stability of laminar natural convection boundary layers, *Prog. Heat Mass Transfer* **2**, 99–124 (1969).
16. R. P. Dring and B. Gebhart, A theoretical investigation of disturbance amplification in external laminar natural convection, *J. Fluid Mech.* **34**, 551–564 (1968).
17. R. P. Dring and B. Gebhart, An experimental investigation of disturbance amplification in external natural convection flow, *J. Fluid Mech.* **36**, 447–464 (1969).
18. C. Heiber and B. Gebhart, Stability of vertical natural convection boundary layers: some numerical solutions, *J. Fluid Mech.* **48**, 625–646 (1971).
19. Y. Joshi and B. Gebhart, Transition of transient vertical natural convection flow in water, *J. Fluid Mech.* **179**, 407–438 (1987).
20. A. J. A. Morgan, The reduction by one of the number of independent variables in some systems of partial differential equations, *Q. J. Math., Oxford Science Series* **3**, 250–259 (1952).
21. S.-F. Shen, Some considerations on laminar stability of time-dependent basic flows, *J. Aerospace Sci.* **28**, 397–404 (1961).
22. B. Gebhart and R. Mahajan, Instability and transition in buoyancy-induced flows, *Adv. Appl. Mech.* **2**, 231–315 (1982).
23. J. A. Adams and D. F. Rogers, *Computer-aided Heat Transfer Analysis*, Appendix B. McGraw-Hill, New York (1978).
24. F. M. White, *Viscous Fluid Flow*. McGraw-Hill, New York (1974).